Building and Environment 234 (2023) 110102

Contents lists available at ScienceDirect

Building and Environment

journal homepage: www.elsevier.com/locate/buildenv

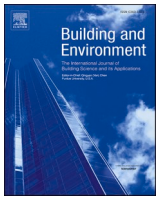

Thermal characterization of a modular living wall for improved energy performance in buildings

Zaloa Azkorra-Larrinaga *, Aitor Erkoreka-González, Koldobika Martín-Escudero, Estibaliz Pérez-Iribarren, Naiara Romero-Antón

ENEDI Research Group, Department of Energy Engineering, University of the Basque Country (UPV/EHU), Torres Quevedo 1, 48013, Bilbao, Spain

ARTICLE INFO

Keywords:
Modular living wall
Vertical greenery
Energy performance
Energy saving
PASLINK test Cell

ABSTRACT

Vertical vegetation systems are an innovative passive method for decreasing the thermal energy demand of buildings while increasing the quality of urban life. The main objective of this work is to calculate the effectiveness of vegetation in reducing thermal loads analytically. For this purpose, the thermal energy performance of the modular living wall was compared with a traditional double façade construction system to evaluate the influence of vegetation using Stochastic Differential Equations models.

The research was carried out experimentally using a real-scale PASLINK test cell. The thermal behaviour of a double leaf bare wall and the same double leaf wall converted into a modular living wall were calculated for different summertime and wintertime periods. In both studied cases, the temperature of the exterior surface of the bare wall is taken at the same place regardless of whether or not there is greenery system in the energy balance. With this simplification, the effect of the modular living wall can be identified within the estimated coefficients.

The thermal resistance of the conventional double façade increased 0.74 (m^2 K)/W over the non-greened wall, which represents a weighted increase of 49%. Additionally, the experimental results showed that the evapotraspiration processes that take place in the living wall lead to an increase in the combined convection-radiation coefficient, which reduces the overheating of the façade. Moreover, the effective solar absorptivity value of the outermost surface of the bare wall has been reduced an 85% thanks to the living wall, which confirms the high capacity of the living wall to reduce solar heat gains.

1. Introduction

Historically, architecture and construction have been based on experience and knowledge of the environment and climate. After a period in which building design ignored the local climate, buildings have emerged that incorporate passive techniques into architecture, achieving buildings with low energy needs [1]. In addition, using less energy reduces greenhouse gas emissions and reduces operating costs [2].

The useful life of a building can be prolonged by acting on the envelope since it is the part of the building that suffers from inclement weather and the one that, together with the facilities, are responsible for the thermal comfort of the dwellings [3]. By acting on the envelope, a significant improvement in living conditions can be achieved by reducing CO_2 emissions and energy demand [4].

For some time now, one of the systems used to improve the thermal resistance of building façades is the Living Walls (LW). The LW are new building components that allow for the greening of the façades of cities. LW can be formed by geotextile felts, modules and/or panels, fixed to vertical supports or the wall structure itself [5]. Among numerous benefits, such as urban heat island mitigation [6,7], reduction of greenhouse gas emissions [8,9], reduction of road traffic noise [10,11], improving air quality [12,13], is reducing building envelope outermost surface temperature, the most significant benefit of LW which yields building energy savings [14–19].

Through the use of the LW, the temperature reduction on the external surface of the building is achieved. This reduction in temperature in the outermost layer of the building is considered an approximation of the potential of these passive systems for energy saving [20–23]. Temperature reduction occurs through shading and insulation by vegetation and substrate, evaporative cooling by evapotraspiration and, finally, the wind barrier effect [24,25].

Another aspect that needs to be considered is the effect that

* Corresponding author.
E-mail address: zaloa.azkorra@ehu.eus (Z. Azkorra-Larrinaga).

https://doi.org/10.1016/j.buildenv.2023.110102
Received 25 October 2022; Received in revised form 8 February 2023; Accepted 13 February 2023
Available online 15 February 2023

Abbreviations

Nomenclature

A	area (m^2)
C	effective heat capacity (kJ/(m^2 K))
Gv	global solar radiation on a vertical plane (W/m^2)
h	convective heat transfer coefficient (W/(m^2 K))
k	thermal conductivity (W/(m K))
Q	heat flow (W)
q	heat flow density or heat flux (W/m^2)
R	thermal resistance ((m^2 K)/W)
T	temperature (°C)
U	thermal transmittance (W/(m^2 K))

Greek symbol

α	absorptivity (−)

Subscripts

c	air space or air camera
e	exterior air ambient
i	indoor air ambient
s	surface (homogeneous layer outer surface)
se	exterior surface of the base wall
w	wall

Abbreviations

BW	Base wall
GF	Green façade
GR	Green roofs
LCCE	Laboratory for Quality Control in Buildings
HF	Heat flux sensor
LW	Living wall
MLW	Modular Living Wall
PAS	Pseudo-Adiabatic Shell
PRBS	Pseudo Random Binary Sequence
SDE	Stochastic Differential Equations
VGS	vertical greenery systems

vegetation has on the building envelope thermal resistance, this needs to be considered, as demonstrated by Ref. [26] in a numerical investigation.

The thermal effect of vegetation and its cooling potential for buildings has been widely studied in the last few decades. The choice of modelling tools and study design depends on several factors, both internal (plant species, foliage density and type of greenery system) and external (wall orientation, wall layer composition, climate and season).

To assess the real thermal performance of vertical greenery systems (VGS), it is necessary to obtain a reliable in-situ thermal characterization instead of theoretical design values. Therefore, the main limitation for characterising in-situ measurements is the dynamic exterior climatic conditions. Numerous studies on vegetated façades are based on in situ measurements to evaluate the wall's thermal performance and energy savings. Ottelé and Perini [27] present a comparative thermal analysis of a LW versus a Base Wall (BW) where the contribution of the vegetation to the thermal performance of the building envelope is quantified, reducing the building envelope temperature by 8.4 °C. Coma et al. [28] compared, on a real scale, the thermal performance of two different vertical greenery systems for a whole year. The results showed the effectiveness of the vegetal solution for energy savings during the cooling season. Blanco et al. [16] evaluated the energy analysis of a green façade under different summertime weather scenarios. A comparison was carried out on the energy transfer at the covered wall, behind the vegetation, and at an un-vegetated wall. The surface of the walls, the air gap in the green façade and the external air temperature measurements showed that the green façade provided a reduction in the wall surface temperature of up to 9.9 °C. Another study by Daemei et al. [29], based on in situ measurements and simulations considering the same parameters for a vegetated façade and bare wall, stated that, after measurements, the green wall dropped the indoor temperature by 9% and decreased the relative humidity level by 32%. Bano and Dervishi [30] used numerical and experimental approaches to evaluate the thermal performance of the vegetated façade in a hypothetical 20 stories high-rise office building. A test of greenery systems was applied in façades with different window-to-wall ratios. The results showed the efficiency of vegetation strategies on opaque walls achieving a significant range of energy reduction from 9% up to 11% for 50% window-to-wall ratio scenarios for the Mediterranean climate. Fox et al. [31] focused on the thermal performance provided by a living wall, measuring the heat flux through a pre 1970s uninsulated cavity masonry wall construction that was retrofitted with an external LW system face and compared with an identical wall built-up on the same elevation without the living wall cladding. The results found that the thermal transmission value for the pre-1970s wall, with an additional LW façade cladding, was 31.4% lower than that of the same wall without the LW (from U-value for cavity masonry wall without the living wall façade 1.12 W/(m^2 K) to 0.77 W/(m^2 K) with the living wall façade).

Another aspect to consider is the mathematical modelling of vegetated façades; Kontoleon and Eumorfopoulou [32] created a building scale lumped thermal-network model and used it to simulate the thermal performance of VGS for several wall orientations, plant cover and positions of a wall insulation layer. Kenai et al. [33] presents a numerical simulation of the energy effect of a solar mask created by a green wall on the thermal performance of a building envelope in a temperate climate. He et al. [34] developed and validated a coupled heat and moisture transfer model to examine the thermal performance of a LW in summer and winter. In these examples, the impact of orientation on relative thermal benefits of LW was analysed, and the equivalent thermal resistance was calculated.

Flores et al. [35] provided an application example on a building prototype with a green façade that was simulated through EnergyPlus software. This method has been applied by Daemei et al. [29]. In this way, Hao et al. [36] found that the experimental data from a vegetated test cell agree with the simulated data with EnergyPlus. They focused their study on the indoor operative temperature and the interior wall surface temperature; concluding that the energy saving due to GW is 7–8%. García et al. [37] developed a LW heat and mass transfer model coupled to EnergyPlus through the Matlab-Energyplus Co-Simulation Interface (MLE) toolbox to simulate the heat transfer between a building and several vegetative surfaces simultaneously. Their study concludes that the cooling load reduction of living walls is 19.7–24.9%, while green roofs show a lower reduction of 9.6–15.1%. Results show that in summer the green wall reduced heat gains from the façade by 97% while heat losses were reduced by 30%. Furthermore [38], deals with the full monitoring of an experimental green wall set up; the results underline the positive effect of green walls in summer and show a moderate reduction in heat losses in winter.

A correct and complete monitoring system of vegetated façades is critical for their experimental thermal characterization. At present, despite numerous studies to assess the impact of vegetation on the energy performance of existing buildings, no long-term tests (2 years) have been carried out under exterior climatic conditions with quality and highly controlled measurement conditions, as applied in the test methodology of the PASLINK test cells. Such is the case of this study.

The sample energy performance has been modelled using Stochastic

Differential Equations (SDE). The SDE are connected to data through a state-space formulation consisting of continuous-time state equations and discrete-time observation equations. The aim of the work is to simplify the mathematical model so that such complicated parameters as (h_{se}) combined convection and radiation coefficient between the external surface of the façade and the external environment and (α) solar absorptivity can be identified with a simple equation. Therefore, the model developed in this research offers an advance over previous models by calculating such wall characteristics, as the thermal resistance and capacitance and equivalent solar absorptivity. These dynamic data analysis methods based on system identification techniques can be applied to building energy simulation calculations. In this sense, this research is promising, and could help to develop models that may be used to quantify the energy savings achieved with VGS in any other location with different ambient conditions.

With the mathematical model and the results obtained from the two façades analysed (BW and MLW), the impact on the energy efficiency of MLW can be evaluated, thus making it possible to quantify the energy improvement of buildings with and without VGS.

2. Material and methods

2.1. Climatic conditions

The experimental site is located in Vitoria-Gasteiz, Araba, in the north of Spain, in the facilities of the Laboratory of Quality Control in Buildings of The Basque Government (LCCE), (latitude: 42° 51′N, longitude 2°41′W) under an oceanic climate situation defined as Cfb (warm temperature, fully humid, warm summer) according to the Köppen and Geiger climate classification [39]. The climate is warm and temperate, with much rainfall, even in the driest month. The temperature average is 12 °C, and the precipitation average is 855 mm.

2.2. Experimental setup

The development of the experiment was carried out in a PASLINK test cell (see Fig. 1). The objective of the PASLINK test cell and analysis procedures is to obtain the thermal characteristics of building components under real dynamic conditions. Since the beginning of the PASSYS Project in 1985, the analysis and testing methodology and software tools have evolved and improved the accuracy of both measurements and results [40].

The PASLINK test room has the dimensions of an average room in a European house, so it is suitable to obtain results comparable to the real conditions of a building, but with the advantage that it is fully controlled without occupancy effects. On the one hand, it is divided into two sections; the service room, where the instrumentation necessary for measuring and controlling the tests is located; and on the other hand, the test room with dimensions of 5 *m* in length with a square section of 2.7 *m* on each side (the communication points between both rooms are perfectly controlled to minimise possible uncontrolled or quantified heat leaks, while minimising measurement errors).

The test cell acts as a calorimeter that allows the exchanged heat fluxes, both gains and losses, between the controlled interior environment and the exterior to be measured with a high precision. It is formed by highly insulating walls, except on the study surface, where the sample is placed to be tested (south façade).

2.3. Description of the evaluated façades

This research aims to compare a bare double-leaf wall (Base Wall or BW) with and without a MLW to quantify the contribution of vegetation to the thermal performance of the analysed BW solution. Both systems, BW and BW with MLW, were placed on the south façade of the PASLINK test cell.

2.3.1. Base wall description

The double-leaf BW (see Fig. 2) consists of a double-sided vertical enclosure made from inside to outside by the following layers.

The dimensions of the sample were 2.7 × 2.7 m (sample area 7.3 m^2).

2.3.2. Modular living wall description

The MLW (see Fig. 3) is placed on the double-leaf BW *(Layer 1–4);* it consists from inside to outside of the following layers: *Layer (5),* the ventilated air chamber (5 cm) is situated between the BW and the pots. It contains a metallic substructure based on stainless steel profiles attached to the wall using metallic screws. *Layer (6)* the internal part of the squared pots 60 cm × 40 cm x 8 cm thick, made of recycled polyethylene. MLW are extreme gardens, as they have a steep slope and limited soil volume, leading to potential drought stress. Because of this, every module has four micro automatic irrigation tubes installed on the top and two down for drainage. The irrigation system includes a recirculating system where the excess water and nutrient solution is recuperated at the bottom of the MLW, stored in a tank, and pumped again for irrigation. *Layer (7)* Coconut fibre as substrate inside the module. *Layer (8)* the outer part of the squared plots. *Layer (9)* the external layer is a shrub (*Helichrysum italicum*) that was selected in this test to guarantee the uniformity of the vegetal façade and because it is well adapted to survive in cold winters.

2.4. Measurement campaign

In order to characterise the thermal characteristics of the MLW located on the double-sided vertical BW, different actions were carried

a) b) c)

Fig. 1. PASLINK test cell in LCCE a) Detail of the MLW on the south wall of the PASLINK test cell. b) Detail of the service room; partition door and data acquisition and control system can be seen c) Detail of the interior of the test room without the south-facing sample.

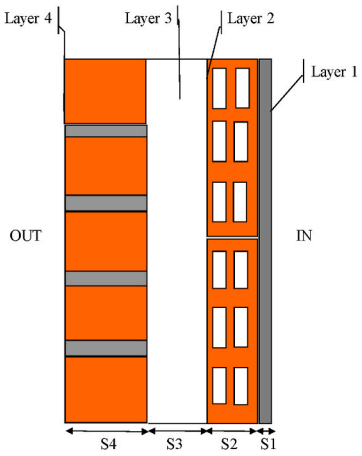

- Surface 1: thick cement mortar (1.5 cm)
- Surface 2: double hollow brick (32 cm x 14 cm x 6.4 cm thick).
- Surface 3: not ventilated air chamber (10 cm)
- Surface 4: perforated brick (22.8 cm x 49 cm x 10.5 cm thick).

Layer 1: internal part of the surface 1
Layer 2: external part of the surface 2
Layer 3: not ventilated air chamber
Layer 4: external part of the surface 4

Fig. 2. Representation of the constructive system in the experimental setup in the PASLINK test cell. Double-leaf base wall (BW) surfaces and layers.

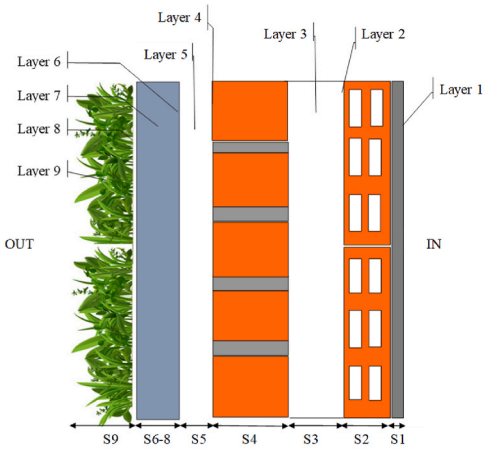

- Surface 1-4: Double-leaf Base Wall (BW)
- Surface 5: not ventilated air chamber (5 cm)
- Surface 6-8: Modular Living Wall structure and module plus substrate (60 cm x 40 cm x 8 cm thick)
- Surface 9: Evergreen shrub

Layer 1: internal part of the surface 1
Layer 2: external part of the surface 2
Layer 3: not ventilated air chamber
Layer 4: external part of the surface 4
Layer 5: Ventilated air chamber (5 cm)
Layer 6: internal part of the surface 6-8
Layer 7: substrate
Layer 8:external part of the surface 6-8
Layer 9: evergreen shrub

Fig. 3. Representation of the constructive system in the experimental setup in the PASLINK test cell. Modular Living Wall (MLW) surfaces and layers.

out. The first took place in June and July 2012. The assembly and monitoring of the double-sided vertical BW façade were carried out. As the thermal characterization of a conventional façade (BW) does not depend on the annual period of the test, no wintertime tests were carried out to maximise the LW test period.

During six months, the evergreen plants grew in the modules and were subsequently attached to the BW when the measurement campaign was ready. The LW was installed on the BW and monitored from 1st January 2013 to 31st December 2014 to compare the improvement in energy rehabilitation based on a construction element, in this case, a double-leaf BW.

For this purpose, the test room indoor air was excited with heat inputs following a Pseudo Random Binary Sequence (PRBS). The PRBS are low-frequency sequences explicitly created in the PASLINK project to obtain high-quality data sets suitable for dynamic model calibration [40]. This signal is used for two reasons. Firstly, it allows data sets containing information about the low-frequency response of the tested components to be obtained. Secondly, as the heat input signal is completely uncorrelated with the external environmental conditions, the parameters can be identified under optimal conditions [41].

Replication is often a problem in exterior tests or monitoring, as most measurements are carried out only once under the same conditions. The methodology of a PASLINK test cell made it possible to repeat the test several times and obtain traceable results. In the case of the BW, the study was repeated twice; and in the case of the MLW, four times, three during wintertime and once in summertime. It should not be forgotten that the ultimate goal is the use of MLW in urban design and the rehabilitation of poorly insulated grey walls in cities so that green walls can cool the inside of buildings. The façades, test series and dates are shown in Table 1.

2.5. Measurement devices

This section describes the measurement sensors and their accuracy. In order to make the comparison between the BW with and without vegetation, it is necessary to measure the difference through the building envelopes under similar season weather conditions; therefore, good monitoring is necessary.

The instrumentation and monitoring of data collection in the PASLINK test cells were carried out under the requirements established in

Table 1
Façade, test series and date of data set analysed.

Façade	PRBS Series	Date
BW	SEC I	22/06/2012–30/06/2012
	SEC II	06/07/2012–13/07/2012
LW	SEC III	07/01/2013–17/01/2013
	SEC IV	29/01/2014–04/02/2014
	SEC V	09/07/2014–18/07/2014
	SEC VI	09/12/2014–16/12/2014

the measurement and calibration manuals for PASLINK cells [42–44]. In the same way, all the necessary sensors (temperature, heat flux, solar radiation, humidity, air direction and airspeed) (see section 2.3) were installed, complying with the specifications of the PASLINK manuals.

The following list summarises the sensors used within the sample throughout the trials (see Fig. 4 and Fig. 5). In order to evaluate the thermal performance of the different studied construction systems, the following data were recorded every minute, and the measurements were averaged every 10 min.

- Internal and external surface temperature: The temperature of every layer was monitored using an A-class Pt-100 probe (±0.1 °C). Every layer of the façades were monitored with four probes each. In every layer, there were probes at three different height levels.
- Internal ambient temperature: The temperature inside the test room was measured at seven points using platinum thermoresistances (Pt100) with an accuracy of ±0.1 °C.
- Air temperature and velocity in the air chamber: The profile of the air velocity along the height of the ventilated layer (*Layer (5)*) was measured by four air velocity sensors (±0.1 m/s) placed inside the air gap.
- Heat flux: Every layer of the samples has a Heat Flux sensor, model HF-01, manufactured by Hukseflux, the accuracy was 5% and the voltage was measured directly using a differential connection. All the Heat Flux sensors have been placed in the central part of every layer that makes up the façade, and opposite each other on both sides of each layer, to measure the variation of heat flux crossing the tested samples. In this way, it is possible to neglect the edge effects and assume a one-dimensional heat flux model.
- Electric consumption: To ensure that heat flowed outward from the cell, the electric heating power of 400 W was used for the PRBS sequence pulses within the test room. This power consumption was measured using a power transducer (±0.5 W).
- The vertical global solar radiation incident on the plane of the tested MLW was recorded using a Kipp&Zonen CM11-P pyranometer (measurement accuracy ±3%).
- A meteorological station was installed in front of the PASLINK test cell with the following sensors: exterior air temperature was measured with a platinum thermoresistance Pt100 (measurement accuracy ± 0.1 °C) protected against radiation and mechanically ventilated; the relative humidity was measured with an AHLBORN FHA 646 E1 sensor (measurement accuracy ±2%).

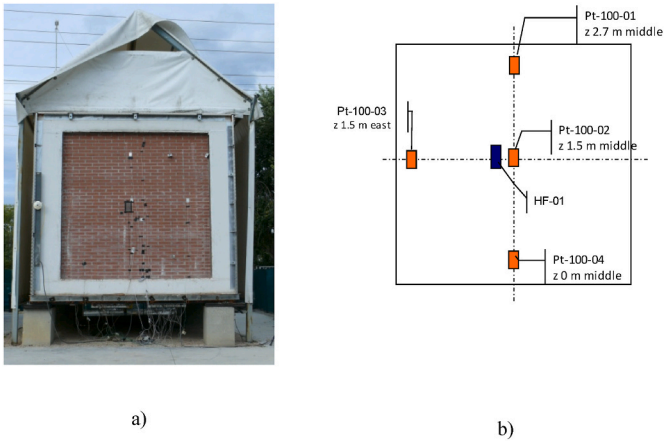

Fig. 4. a) Detail of the position of the sensors on the experimental Base Wall (BW) external surface (Layer 4) b) Front view representation of the common sensors placed in all the layers (BW and LW), sensor type and position. (Pt-100: surface temperature sensors Pt-100-01: z = 2.7 *m* middle; Pt-100-02: z = 1.5 *m* middle; Pt-100-03: z = 1.5 *m* east and Pt-100-04: z = 0 *m* middle and HF: heat flux sensor).

All sensors were calibrated and connected to the Agilent 34970A data acquisition system.

2.6. Data acquisition

2.6.1. Data of the base wall

The measurement data of the double-leaf BW is shown below. Fig. 6 shows the measured data of the PRBS sequence carried out during SEC I together with the temperature fluctuations of the different layers that make up the BW façade associated with it. It is possible to check how the temperature of the inside of the PASLINK cell and that of the first layer responds immediately to the heat pulses of the electric resistance. The PRBS sequence induces changes completely independent of the day/night cycle inside the cell. Both the indoor air temperature and Layer 1 follow this sequence. On the other hand, the outermost layers show day/night temperature oscillations that closely resemble the temperature changes occurring outside, correlated also with global vertical south solar radiation (G_v).

The days shown in this figure were sunny (except on 27 and 30 June), and the average peak global solar irradiation was 500 W/m^2. On hot summer days with high radiation (the façade is south facing), the air temperature is lower than the last layer of the BW due to the solar energy stored in the BW layers. The surface temperature of the façade rises to a high level when solar radiation appears and cools down again when the radiation disappears. Due to the high inertia of the wall during the night and the heat generated within the test room, the temperature of the last layer does not cool down below the ambient temperature. For example, from 25 to 28 June, Layers 4 and 3 maximum values were above 40 °C, while the outside air was at a maximum of 34 °C.

Fig. 7 illustrates the evolution of the main environmental variables affecting the heat flow through the tested sample, together with the indoor air temperature and the heat fluxes across different layers of the sample during this period.

2.6.2. Data of the modular living wall for the summer season

One of the measurements performed during the summer season (SEC V), during the month of July for 10 consecutive days, is shown in detail in Figs. 8 and 9. During this period, the weather in Vitoria-Gasteiz was representative of the climate of this city for summer, located under an oceanic climate. The temperature was often as high as 30 °C in the afternoon and sometimes reached 35 °C. Vertical global solar irradiation reached about 500 W/m^2 on sunny clear days.

One of the effects of the vertical greening system on the exterior surface is that it prevents solar radiation from reaching the base wall, thus ensuring that its outermost surface temperature does not increase (Layer 4). This effect is shown inFigs. 8 and 9, where the outside and inside surface temperatures are presented and compared to the outside air temperature. The surface temperature is even 10 °C cooler than the exterior environment during the day's hottest hours. However, during the night, the maximum difference between the two temperatures is 2 °C, depending on the external conditions. The solar radiation is associated with the outside temperature, which peaks at 36 °C when the solar radiation is maximum; while, when the radiation drops to peak values of 200 W/m^2, the outside temperature takes values close to 20 °C. In both cases, the LW temperature remains stable below exterior air temperatures.

As presented above, it is clear that, under similar conditions, in the last Layer of the BW (Layer 4), the temperature is greater than the temperature of the Layer 4 once the MLW is installed. The maximum temperature recorded during sunny hot days is higher in the BW (Layer 4: 40-43 °C) than the maximum temperature recorded within the MLW (Layer 4: 31-34 °C) at similar values of outside air temperature (31-34 °C). This is the case on 25–28 June (BW) compared to 15–18 July (MLW). The data are comparable because the two construction solutions were tested in the same PASLINK test cell with similar ambient conditions. However, this simple comparison is not the aim of this paper, but

Fig. 5. Details and measurement devices of the constructive system in the experimental setup in the PASLINK test cell. Above: a) Base wall (BW) detail of the double hollow brick and the perforated brick. b) detail of the sensors and their position in Layer 3, the air chamber. c) detail of the sensors in Layer 1, the internal part of the surface 1. Bottom: d) The MLW of the experimental set up with modular metallic sub-structure and sensor positions. e) detail of the irrigation system and the modular pots with vegetation. f) Experimental set-up of the MLW in Vitoria-Gasteiz, Spain.

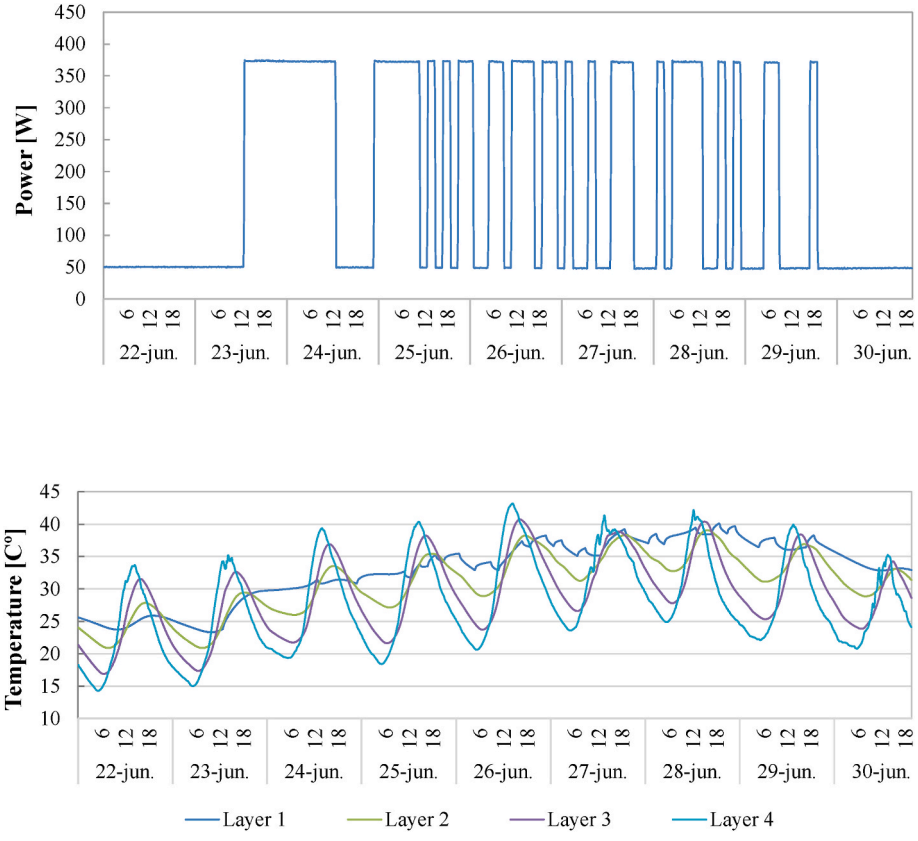

Fig. 6. Above PRBS sequences performed on the BW. Bottom: Evolution of the temperatures in the different layers of the sample during the PRBS sequence (June).

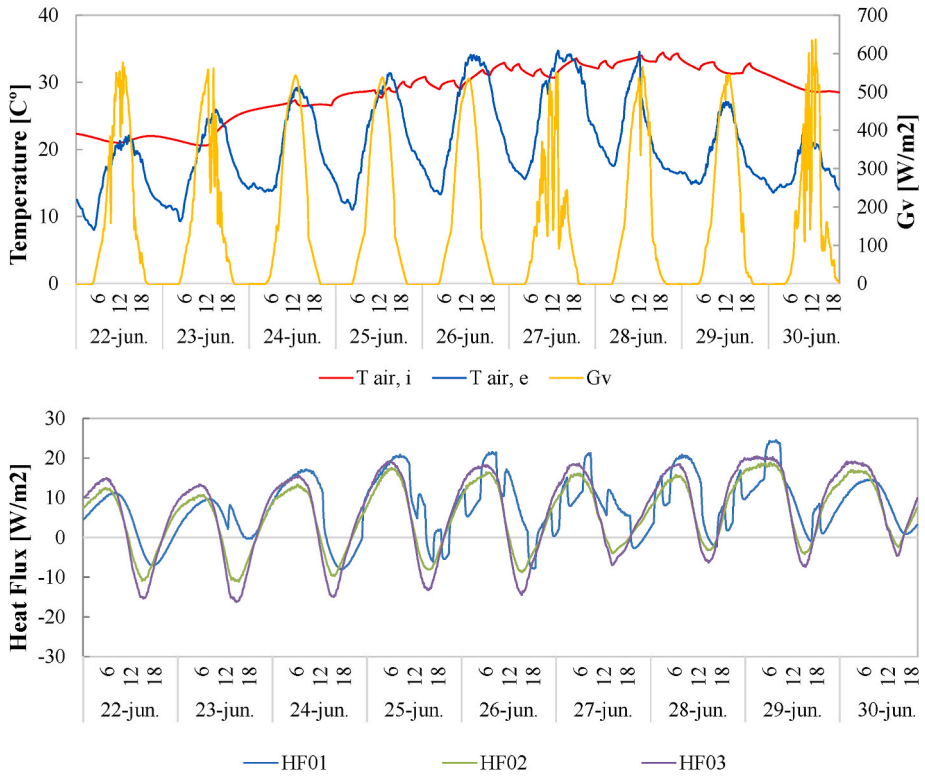

Fig. 7. Above: Evolution of the interior air temperature, exterior air temperature and the south vertical global radiation during the PRBS sequence. Bottom: Evolution of the heat flux sensors in the different layers of the sample (HF01-Layer 1; HF02-Layer 2; HF03-Layer 3) along the PRBS sequence (June).

just to discuss about the validity of the recorded data.

It is evident that the temperature of the MLW is lower than the outside air temperature during the daytime, being the substrate temperature the minimum one. The temperature drops produced by the green wall are more noticeable during the peak hours of heat. In addition, the temperature of the outermost surface of the MLW (Layer 9) is always lower than the exterior air temperature. This decrease in the outermost surface temperature is probably due to the combined effects of evapotraspiration and solar shading.

Focusing on the air temperature in the cavity between the vegetation and the base wall; the air in the cavity had a temperature that was, on average, 5 °C lower in July than the ambient air temperature, resulting in a reduction of energy consumption to keep the indoor air temperature cooled during the summer season.

The heat fluxes are measured by sensors pasted in the centre of all the layers that make up both building solutions (see Fig. 4). InFigs. 7 and 9, the negative values of the heat flux through the façades correspond to heat entering (heat gains), and the positive values correspond to heat leaving (heat losses). The negative heat flux peaks recorded during the day on the façades can be explained by the south orientation of the façades and the direct solar radiation they received. Furthermore, if the heat fluxes conducted through the two façades BW and LW are compared, the figures show that the LW reduces the heat flux transferred through the façade in both directions. The LW, however, reduces heat gains more than heat losses.

2.6.3. *Data of the MLW for the winter season*

During the cold season (winter), the objective was to evaluate whether or not the MLW causes any extra heating consumption in the building caused by the blocking of solar gains. Data on the contribution of these systems in winter (heating season) have been provided by a few authors concerning the external surface temperatures of the building façade wall, with inconsistent results −5.3 °C [28], −3 °C [45] and +0.5 °C [46], respectively.

The following three study periods were carried out during the winter season to achieve this goal. One of the experiment's objectives during the winter season was to assess whether or not the VGS causes a decrease in the temperature of the building façade that may increase heating energy consumption due to the interception of solar gains.

One of the measurements (SEC VI) taken during the cold season for eight consecutive days is shown in detail in Figs. 10 and 11. The data collected during one week in Vitoria are typical of moderately cold weather, as seen in the daily variations of ambient temperature and solar vertical irradiation (Fig. 11). During this period, the diurnal variations of temperature were often between 5 °C and 10 °C, and the vertical global solar irradiation reached about 750 W/m^2 under sunny clear days.

During the PRBS test sequence carried out in the wintertime, a high-temperature gradient is observed between the interior and exterior air; it is over 20 °C. Fig. 11 shows the solar radiation's influence on the exterior air temperature. There are no significant fluctuations in the exterior temperature day/night due to the low solar incidence during this period.

Fig. 11 shows that, compared to the summer measurements, the temperature differences between the façades are minor during the day and more significant during the night. As can be verified, according to the obtained results, the MLW showed a slight reduction in the exterior temperature for the heating period. The MLW mitigates the façade temperature by 2 °C during the day and the night; it remains almost the same as the ambient temperature. This could be attributed to its night time radiative protection (insulating effect) provided by the modules filled with coconut fibre. The MLW ensures that the external surface of the façade radiates less energy to the sky, whereas the BW (Reference) façade has a direct wall exposition to the sky.

During the winter season, the MLW is ineffective in reducing the heating demand, as the constant evapotraspiration of the plants, which is lower than in summer periods, causes a reduction in the temperature of the external layer of the façade (Layer 4). Consequently, adding a

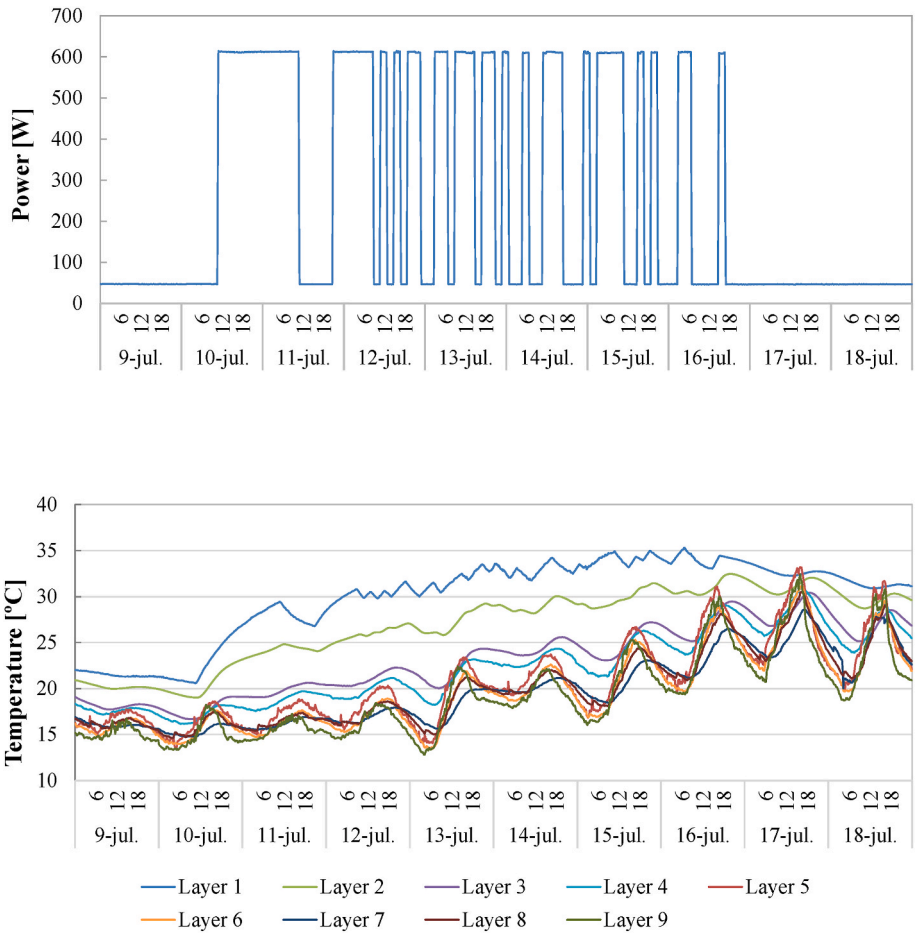

Fig. 8. Above PRBS sequence performed on the MLW. Bottom: Evolution of the temperatures in the different layers of the sample during the PRBS sequence (July).

layer of insulation on the BW prior to the plant system would be advisable if an envelope is to be renovated to reduce heat losses. Therefore, it could be stated that the incorporation of MLW on the façades of a building does not penalise the thermal behaviour of this building during winter periods because no significant advantages were found in the use of the MLW during the heating period.

3. Dynamic characterization model (stochastic state-space modelling)

In this case, a detailed numerical SDE model was used to thermally characterise and evaluate the energy performance of two different façades (BW and MLW). It is a grey-box model consisting of a set of SDE coupled with a set of discrete-time observation equations, which describe the dynamics of a physical system and how it is observed. This type of model represents dynamic systems, where the dynamics are continuous and, at the same time, subject to effects of randomness, while the measurements are discrete.

The CTSM-R [47] software was used to estimate and identify physical systems. The parameters of the models were estimated using the Continuous-Time Stochastic Modelling (CTSM-R) toolbox implemented in the statistical software R.

Two hidden state stochastic grey-box models were used to identify and characterise the thermal resistance of the façade components under study (BW and MLW). The grey box model builds physical models based on dynamic data of the building components by adjusting the behaviour of these models to the measured heat fluxes through the components and with the climatic variables. The mathematical RC model represents the façade elements, consisting of thermal resistances and capacitances that detail the heat transfer through the layers that make up the building element as a set of continuous stochastic differential equations formulated in state-space form [48].

3.1. Model for the BW

The basics of heat transfer are indicated, followed by the introduction of the mathematical tools of the dynamic method, which allow the identification of the thermal parameters. For the calculation of the wall surface temperature, the following assumptions have been made. First, it is supposed that the façade is homogeneous and that all the significant heat flux through the wall is one-dimensional and perpendicular to the wall surface.

The dynamic thermal parameters depend on the physical characteristics of the materials that make up the building envelope. Fig. 12 shows the variables in the heat energy balance through the wall with two hidden state variable models.

The coupling of the different elements of the model is presented in Fig. 13. Connection with the outdoor environment is through thermal resistances and temperature–capacity nodes. Solar gains on the envelope outdoor surface were also taken into account. The thermal resistances are presented, R_{se}, R', R_2 and R_1. Where, h_{se} ($R_{se} = 1/h_{se}$) is the exterior surface heat transfer coefficient, which contains convective and long-wave radiative components, representing the combined coefficient of heat transfer by convection and radiation between the outer surface of the façade and the exterior. C_2 and C_1 represents the heat capacity of the envelope, C_{se} is the effective capacity of the wall outermost surface (assuming it is massless $C_{se} = 0$), and interior air temperature T_i and a heat capacity of the indoor air mass C_i represent the indoor

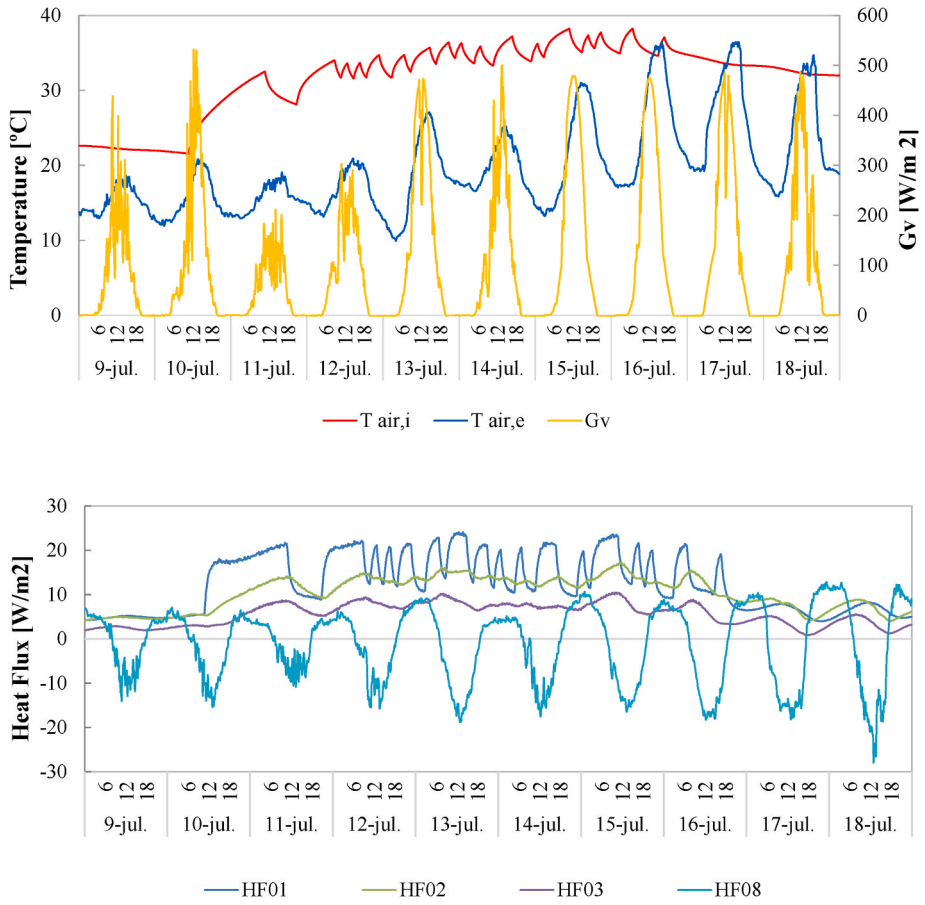

Fig. 9. Evolution of the interior air temperature, exterior air temperature and the vertical global radiation during the PRBS sequence. Bottom: Evolution of the heat flux sensors in the different layers of the sample (HF01-Layer 1; HF02-Layer 2; HF03-Layer 3; HF08-Layer 8) along the PRBS sequence (July).

environment.

Under these assumptions, applying the energy balance to the C_1, C_2 and C_{se} nodes of the BW:

$$C_1 \frac{dT_1}{dt} = \left[\frac{1}{R_2}(T_2 - T_1) + \frac{1}{R_1}(T_i - T_1)\right] \quad \text{Eq. 1}$$

$$C_2 \frac{dT_2}{dt} = \left[\frac{1}{R_2}(T_1 - T_2) + \frac{1}{R'}(T_{se} - T_2)\right] \quad \text{Eq. 2}$$

$$C_{se} \frac{dT_{se}}{dt} = 0 = \left[\frac{1}{R'}(T_{se} - T_2) + \frac{1}{R_{se}}(T_e - T_{se}) + \alpha G_v\right] \quad \text{Eq. 3}$$

Eq. (3) is developed as follows:

$$0 = \left[\frac{1}{R'}T_2 - T_{se}\left(\frac{1}{R'} + \frac{1}{R_{se}}\right) + \frac{1}{R_{se}} T_e + \alpha G_v\right] \quad \text{Eq. 4}$$

Being $R_3 = R_{se} + R'$

$$T_{se} = \left[\frac{R_{se}}{R_3} T_2 + \frac{R'}{R_3} T_e + \frac{R' R_{se}\, \alpha}{R_3} G_v\right] \quad \text{Eq. 5}$$

Entering T_{se} value in Eq. (2) and being $R_{se} = 1/h_{se}$

$$C_2 \frac{dT_2}{dt} = \left[\frac{1}{R_2}(T_1 - T_2) + \frac{1}{R'}\left(\frac{R_{se}}{R_3 R'}T_2 + \frac{R'}{R_3}T_e + \frac{R\acute{R}_{se}\,\alpha}{R_3 R'}G_v - \frac{T_2}{R'}\frac{R_3}{R_3}\right)\right] \quad \text{Eq. 6}$$

$$C_2 \frac{dT_2}{dt} = \left[\frac{1}{R_3}(T_e - T_2) + \frac{1}{R_2}(T_1 - T_2) + \frac{\alpha}{h_{se} R_3} G_v\right] \quad \text{Eq. 7}$$

In that way, it is possible to represent Fig. 13 model only with the equations Eq. (1) and Eq. (7), instead of using the three equations Eq. (1), Eq. (2) and Eq. (3). In this way, the RC-1 network of Fig. 13 has been converted into the RC-2 model of Fig. 14.

where: T_e and T_2 are the temperatures of the exterior ambient and the inner node of the wall, respectively, R_3 which represent R_{se} plus R', α is the absorptivity of the wall's outermost surface and G_v is the global vertical solar irradiance incident on the wall's outermost surface.

From the diagram in the corresponding equations can be developed for each state. Where the BW surface temperature is a function of the T_e, T_2, G_v.

In this case, an initial measurement equations, Eq. (8), is available:

$$\dot{q}_i = \frac{(T_i - T_1)}{R_1} \quad \text{Eq. 8}$$

where T_1 and T_2 are the two hidden states. As proven in the mathematical development of Eq. (5) and Eq. (7), α and h_{se}, represent physical parameters occurring in the outermost surface of the BW. Even if these two parameters are not explicitly shown in the RC- 2 scheme model to be calibrated, the two equations that represent the model of RC-2, consider α and h_{se} as the solar absorptivity of the outermost surface of the BW and the combined convective-radiative heat transfer coefficient occurring in the outermost surface of the BW respectively. This aspect is a key issue of the model, since it has been able to hide the variable T_{se} within Eq. (5) and Eq. (7). In this way, if these two calibrated equations are used to simulate the performance of this BW in another climate for some given indoor ambient temperature (this is usually given by standard for the indoor comfort conditions within the building), it would not require to have the usually unavailable T_{se} measurement. Note that the variables T_e and G_v are usually available for any location where we would like to

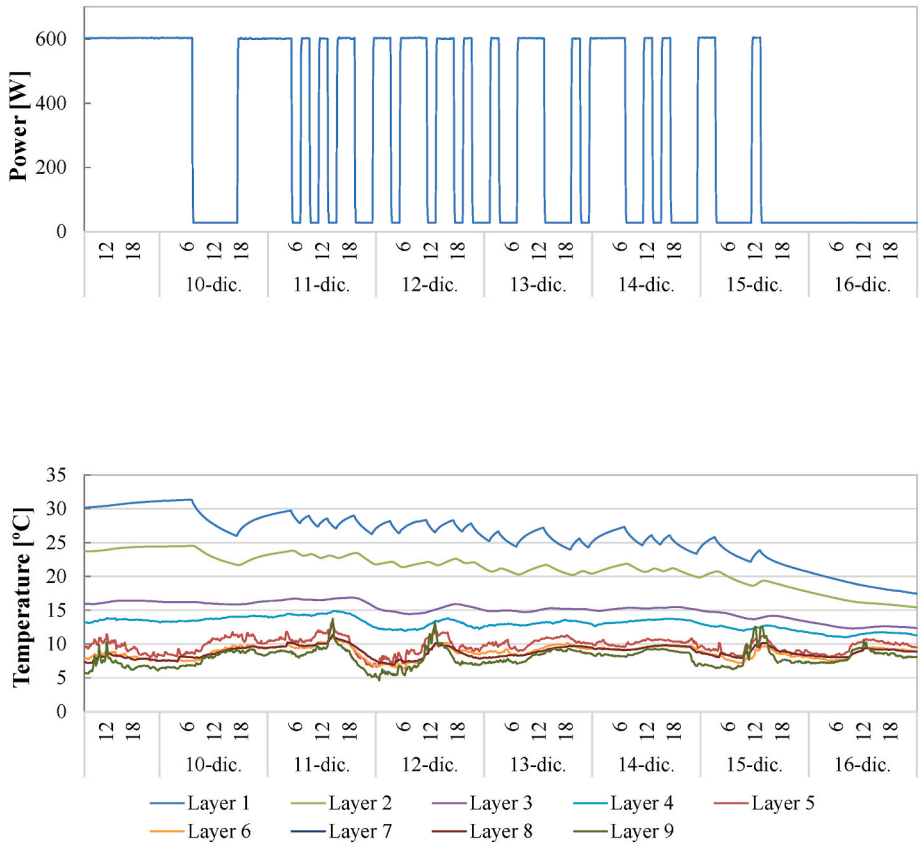

Fig. 10. Above PRBS sequence performed on the MLW. Bottom: Evolution of the temperatures in the different layers of the sample during the PRBS sequence (December).

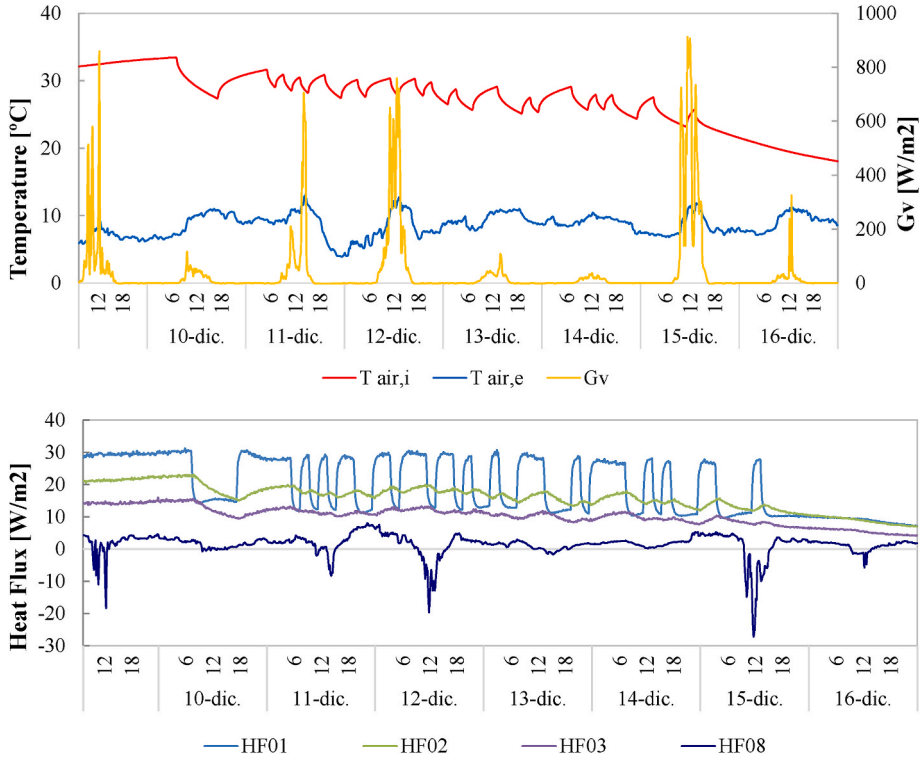

Fig. 11. Evolution of the interior air temperature, exterior air temperature and the vertical south global irradiation during the PRBS sequence. Bottom: Evolution of the heat flux sensors in the different layers of the sample (1HFT01-Layer 1; 1HFT02-Layer 2; 1HFT03-Layer 3; 1HFT08-Layer 8) along the PRBS sequence (December).

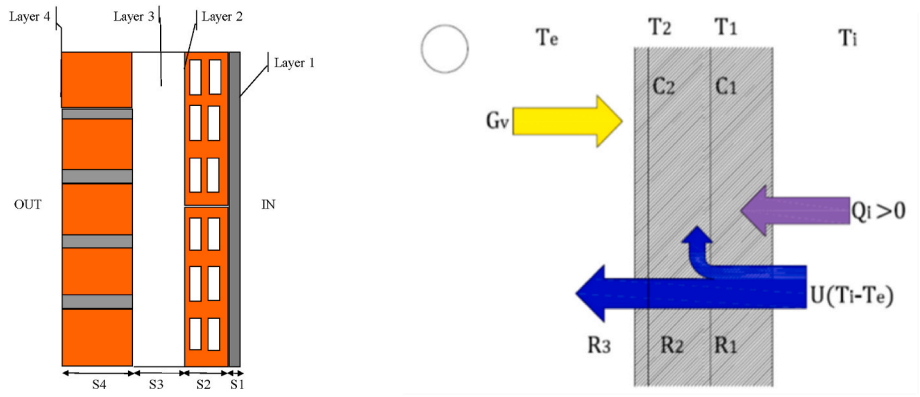

Fig. 12. Representation of the constructive system and the heat flow model of the double-leaf BW considering two hidden states.

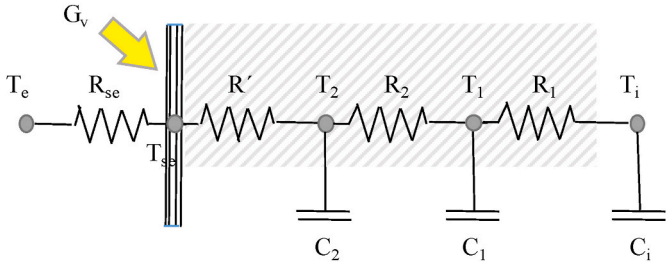

Fig. 13. RC-1 network scheme of the selected model.

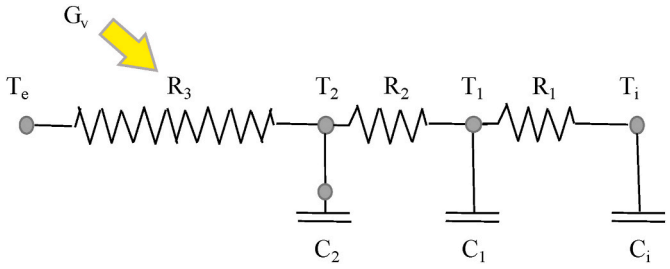

Fig. 14. RC-2 network scheme of the selected model.

simulate the performance of this BW.

Therefore, by these models, it is possible to obtain assessments of the parameters characterising and describing the thermal behaviour of the BW. In the presented models , α and h_{se} can be identified directly.

The effective heat capacity of the BW is obtained by Eq. (9).

$$C = \sum_i C_i A \quad \text{Eq. 9}$$

where C is the effective heat capacity of the BW and A the surface of the BW.

The value of the thermal resistance of the BW is obtained by the equation Eq. (10).

$$R = \sum_i R_i A \quad \text{Eq. 10}$$

where R is the thermal resistance of the BW.

3.2. Model for the MLW

Once the VGS has been installed in the BW outermost surface, with an analogous mathematical development as was done for the BW, an analogous system with two equations has been obtained; Eq. (11) and Eq. (12). The schematic of this modelling approach is shown in Fig. 15 with the parameters and variables involved in the heat energy balance through the façade in the assumption of two hidden state variables.

A model made for the MLW is described by the equations from the schematic in Fig. 15; the corresponding equations can be developed for each of the states Eq. (11) and Eq. (12):

$$C_1 \frac{dT_1}{dt} = \left[\frac{1}{R_2}(T_2 - T_1) + \frac{1}{R_1}(T_i - T_1) \right] \quad \text{Eq. 11}$$

$$C_2 \frac{dT_2}{dt} = \left[\frac{1}{R_3}(T_c - T_2) + \frac{1}{R_2}(T_1 - T_2) + \frac{\alpha}{h_{se} R_3} G_v \right] \quad \text{Eq. 12}$$

where T_1 and T_2 are the two hidden states and the observation equation:

$$\dot{q}_i = \frac{(T_i - T)}{R_1} \quad \text{Eq. 13}$$

Therefore, through this two-equation model, it is possible to obtain assessments of the parameters by characterising and describing the thermal behaviour of the MLW. Since an analogous model to that of the BW is being proposed, α and h_{se} has now lost their physical significance they had for the BW model. However, both α have a similar physical meaning: how much of the global vertical solar irradiance incident on the outermost surface of the MLW ends up being absorbed into the outermost surface of the BW. Note that, for both the BW and the MLW analysed walls, the BW outermost surface has the same physical position (it is the T_{se} position in RC-1 scheme). In the same way, h_{se} represents the combined convection-radiation heat transfer coefficient with respect to the T_c in the outermost surface of the BW. While, for the MLW, the h_{se} represents the combined convection-radiation-shading-evapotranspiration effect occurring in the outermost surface of the BW (again it is the T_{se} position in RC-1 scheme) with respect to the T_c.

As in the BW model, the effective heat capacity of the MLW is obtained by Eq. (14):

$$C = \sum_i C_i A \quad \text{Eq. 14}$$

where C is the effective heat capacity of the MLW.

The value of the thermal resistance of the MLW is obtained by the equation Eq. (15).

$$R = \sum_i R_i A \quad \text{Eq. 15}$$

where R is the thermal resistance of all the MLW.

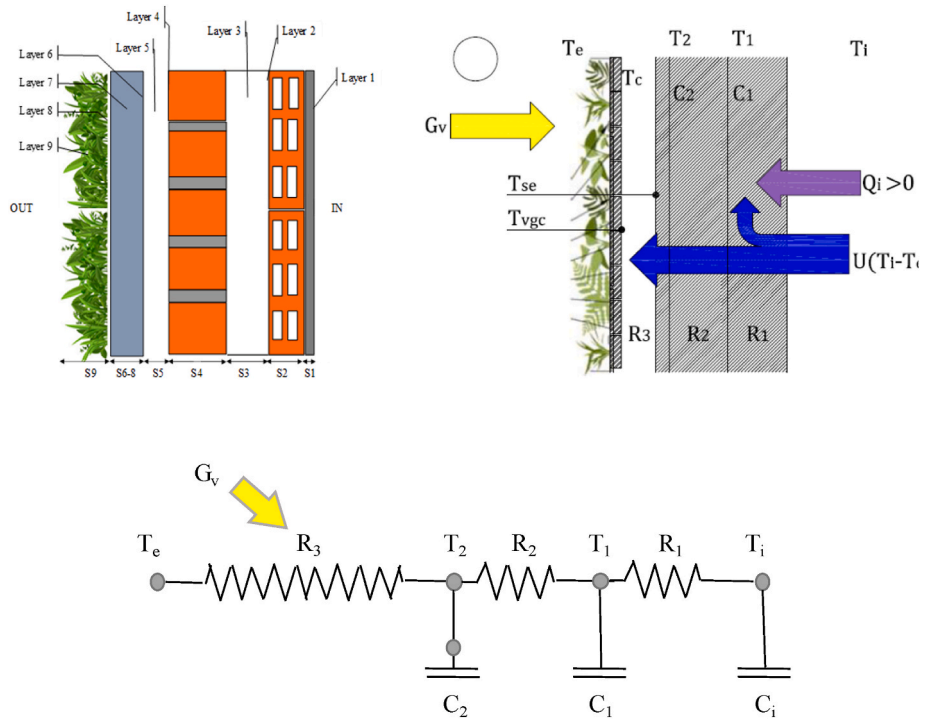

Fig. 15. Representation of the constructive system and the heat flow model of the energy balance in the MLW considering two hidden states.

4. Results and discussion

4.1. Thermal characteristics of the BW

The results obtained from the model with two hidden states used to estimate the characteristic thermal parameters of the BW are summarised in Table 2. No significant differences are observed in the results between the two studied periods. The estimated values of the parameters are within the range of the theoretical values that can be approximately calculated for the BW, with the mean thermal resistance value of 0.77 (m^2 K)/W (non-insulated) and the mean heat transfer coefficient of 6.45 W/(m^2 K).

It is worth noting that the BW is made of double brick and an air chamber without thermal insulation. For this reason, in the case of having the same BW with the addition of 0.06 *m* wide rock wool insulation and a thermal conductivity of 0.04 W/(m K), it would have a thermal resistance of 1.50 (m^2 K)/W, which, added to the resistance of the BW (0.77 (m^2 K)/W), would give a total of 2.27 (m^2 K)/W (moderately –insulated). Therefore, as shown in the data above, implementing an insulation layer will benefit the bare wall, as less energy consumption is needed to keep the indoor air temperature at a comfort level.

4.2. Thermal characteristics of the MLW

Table 3 illustrates the thermal resistance, thermal transmittance, capacitance and absorptivity in each PRBS sequence, calculated using the model with two hidden states for the MLW. The results show consistency between the different analysed series.

Table 2
Results of the thermal characteristics of two hidden states model of the BW for the two different analysed sequences.

Data	R [(m^2 K)/W]	C [kJ/(m^2 K)]	h_{se} [W/(m^2 K)]	α
SEC I	0.75 ± 0.018	252 ± 43	6.68 ± 2.01	0.62 ± 0.37
SEC II	0.79 ± 0.015	291 ± 38	6.22 ± 2.35	0.70 ± 0.79
Average	0.77 ± 0.017	272 ± 41	6.45 ± 2.18	0.66 ± 0.58

Table 3
Results of the thermal characteristics of the two hidden states model for MLW using the four different dates.

Data	R [(m^2 K)/W]	C [kJ/(m^2 K)]	h_{se} [W/(m^2 K)]	α
SEC III	1.47 ± 0.045	366 ± 36	486 ± 31	0.10 ± 0.060
SEC IV	1.54 ± 0.032	305 ± 20	546 ± 23	0.10 ± 0.019
SEC V	1.48 ± 0.013	309 ± 24	135 ± 20	0.11 ± 0.017
SEC VI	1.57 ± 0.017	306 ± 18	458 ± 46	0.10 ± 0.016
Average	1.51 ± 0.026	322 ± 25	[a]497 ± 33	0.10 ± 0.028

[a] h_{se} average data do not consider the sequence taken during the summer season (SEC V).

The thermal resistance (R) value has significantly improved compared to the initial values of the BW (0.77 (m^2 K)/W) (non-insulated) by coupling the MLW (1.51 (m^2 K)/W), which is an increase of the insulating capacity of 49% compared to the initial values. This is a substantial difference from the BW façade. Therefore, the positive effect of using MLW is evident from the heat transmission point of view.

Suppose we return to the case where the BW has a thermal resistance value of 2.27 (m^2 K)/W (moderately –insulated). In this case, by adding the MLW, we would have a total resistance of 3 (m^2 K)/W, which means an increase in the insulating capacity of 32%. Obviously, the insulation effect of the MLW is more significant for less-insulated façades. MLW cannot replace insulation materials, but they can be used as an additional insulation layer for buildings with energy efficiency problems. Therefore, MLW can be applied in new buildings and existing constructions. These results are in line with those found in Refs. [16,27,28,33].

On the other hand, the experimental results showed that the evapotraspiration processes in the MLW increase the combined convection and radiation coefficient, which reduces the overheating of the façade. It is worth highlighting the value of the combined convection-radiation-shading-evapotranspiration coefficient, representing 497 W/(m^2 K) for the sequences taken in the winter periods; however, this value is reduced to 135 W/(m^2 K) in the summer period. An evapotranspiration effect

was also found by [49–51].

Looking at the uncertainty results of the h_{se} heat transfer coefficient parameter in Table 3 (MLW) and Table 2 (BW). It can be seen that it in MLW is lower, probably due to the exterior layer of foliage. The vegetation acts as a windbreak, creating pockets of still air between the leaves, dampening the wind and making convective heat transfer value more constant.

The effective solar absorptivity value is low (0.10), which confirms the capacity of the MLW to reduce solar heat gains and increase the cooling capacity by 85%, compared to the double leaf BW. Analysing the values obtained for the case of the summer season, this is the period of the year when exterior temperatures reach their maximum. At this time, the interest in thermal comfort lies in the cooling effect of the outer layer of the façade. The results prove that the MLW reduces the effective solar absorptivity coefficient of the wall, which leads to a reduction in temperatures on the external layer. The temperature reduction in the outermost layer of the façade has a positive effect on buildings with MLW, making them suitable passive temperature reduction devices. As in the present study, Wong et al. [52] found a 4.36 °C reduction in the average external wall surface in a GF system. A surface decrease of about 4 °C on cloudy days and >6 °C on sunny days was observed by Ref. [53] in the case of direct GF. Lee and Jim [49] registered a smaller fluctuation compared to outside air. They found a diurnal reduction of 9.7 °C and a moderate nocturnal increase of 1.6 °C. Perez et al. [54] found a summer temperature reduction of up to 1.36 °C and, during July, an increase in RH equal to 7%.

Together, these effects result in energy savings for air conditioning and a possible reduction in the urban heat island effect. It can also be observed that a MLW influences the temperature development positively through the façade, resulting in an improvement in the thermal resistance of the building.

4.3. Model evaluation

The residuals from the model were analysed to test whether they can be accepted as white noise. If this is the case, the model describes all the information given in the measurements. The white noise properties are analysed with the autocorrelation functions (ACF) and the cumulative periodograms (CP), plotted in Fig. 16.

The statistical tests show 95% confidence bands under the hypothesis that the residuals for each building component can be considered white noise. Therefore, the statistical tests of the residuals show that the two-state models for the BW and MLW describe the dynamics of the systems. From the results obtained with the different models for the case of the green façade, it can be affirmed that the use of a two-state model correctly estimates the values obtained. However, the analysis of the residues reveals the need to investigate in greater depth and search for alternatives that better explain this enclosure or to obtain models that improve the results obtained and which can be implemented in future studies with the outside temperature, as this would facilitate the simulation and subsequent comparison with other enclosures.

5. Conclusions

The main objective of this research was to compare the thermal behaviour of a non-vegetated Bare Wall (BW) and the same Bare Wall but vegetated with a Modular Living Wall (MLW). For this purpose, a grey-box model was developed in Stochastic Differential Equations and validated using (real) accurate data monitored in an experimental PASLINK test cell located in Vitoria-Gasteiz (Spain). The Stochastic Differential Equations methodology was used to characterise the thermal performance of the MLW and compare it with the thermal performance of the BW. The calculation of the models' residuals with the experimental data allowed the models to be validated. The models obtained from the applied methodology can also be implemented in broader building energy simulation models.

The experimental data show that the modular living wall reduces the temperature on the exterior layer of the building, minimising diurnal heating in particular, and that this effect decreases with an increasing insulation level of the bare wall. Regarding the surface temperature of the modular living wall, the results confirm that the potential cooling effect due to the vegetated surface is significant. The temperature is cooled by 10 °C during summer daytime hours and up to 2 °C during nigh time. As a result of this attenuation, the cooling capacity of the modular living wall and the air cavity immediately behind it can be verified. Therefore, the common use of vegetation and construction insulation materials can develop systems for cooling surfaces that aim at the thermal comfort of its inhabitants and energy savings.

Observing the data of the previous sections, it can be affirmed that while a bare wall, during the periods of maximum radiation, increases its temperature by 20 °C concerning the ambient temperature, the modular living wall maintains the temperature in equilibrium slightly below the ambient temperature. The vegetation does not influence the air temperature, although it is possible to lower the temperature

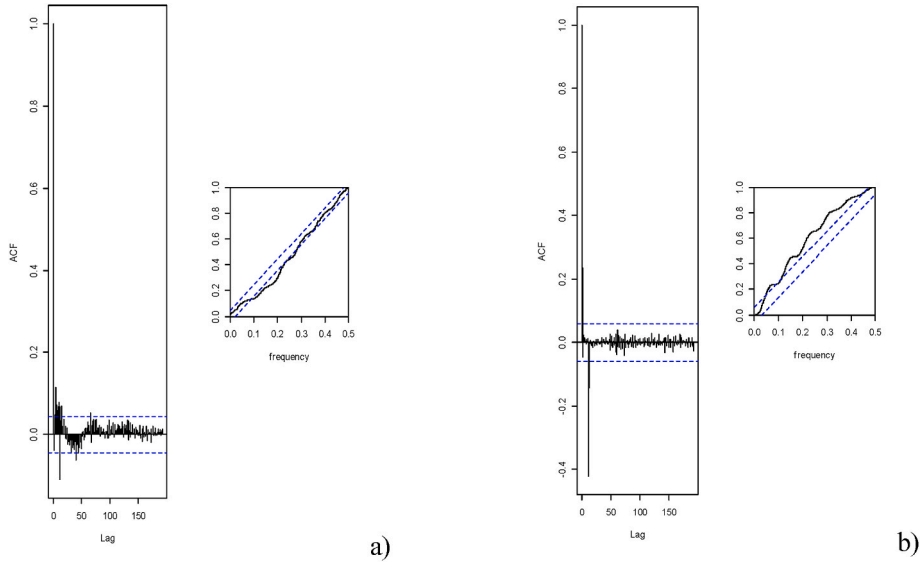

Fig. 16. The auto-correlation function and the accumulated periodogram of the residuals for the selected grey-box model with the two-state model. (a) Bare wall data set SEC I; (b) MLW data set SEC IV.

surrounding the plants through evapotraspiration. If the effect of vegetation is found, it is on surface temperatures; this is due to the shade they exert, thus protecting the air in contact with the surfaces, which does not heat up.

Furthermore, the Stochastic Differential Equations methodology showed that the modular living wall increased the value of the combined heat transfer coefficient in the outermost surface of the BW from 6.45 W/(m^2 K) to 497 W/(m^2 K), reducing the overheating of the façade in the summertime.

The measurements also showed that the effective solar absorptivity of the external surface and the heat flow through the façade was reduced when the modular living wall was applied. The data shows that the cooling capacity of the vegetated façade reduces the solar heat gains in the outermost BW surface by 85% compared to the double-leaf none vegetated façade.

The results of the research represent a contribution to studies on the energy effect of living walls and their modelling, with a special focus on the effect of vertical greenery systems on the energy performance of buildings. α and h_{se}, represent physical parameters occurring at the outermost surface of the BW. A major aspect of the work is that the variable T_{se} can be omitted. Using the equations developed in this article, it is possible to simulate the behaviour of this BW in another climate for a given comfort temperature where it would not be necessary to have the T_{se} measurement. It should be realised that the variables T_e and G_v are usually available for any location where it is desired to simulate the performance of this BW, but T_{se} is generally not available.

Considering the results of this study, the enormous complexity of thermoregulation and plant-façade interaction is evident, dependent on environmental factors and the building solutions, especially the outermost surface and insulation level. The plant's response to solar radiation and its absence has very different daily patterns from the usual inert surfaces of buildings. The most interesting property of the vegetated façade is that these vegetated surfaces maintain their temperature close to that of the air, both day and night, throughout the whole year, making them useful as thermoregulators of thermal exchange.

CRediT authorship contribution statement

Zaloa Azkorra-Larrinaga: Writing – original draft, Software, Methodology, Investigation, Conceptualization. **Aitor Erkoreka-González:** Writing – review & editing, Supervision, Project administration, Methodology, Funding acquisition, Conceptualization. **Koldobika Martín-Escudero:** Writing – review & editing, Supervision, Methodology, Conceptualization. **Estibaliz Pérez-Iribarren:** Writing – review & editing, Software, Methodology, Conceptualization. **Naiara Romero-Antón:** Writing – review & editing, Software, Formal analysis, Conceptualization.

Declaration of competing interest

The authors declare that they have no known competing financial interests or personal relationships that could have appeared to influence the work reported in this paper.

Data availability

Data will be made available on request.

Acknowledgements

This publication is part of the R+D+i project PID2021-126739OB-C22, financed by MCIN/AEI/10.13039/501100011033/ and "ERDF A way of making Europe".

This project has been made possible thanks to the agreement between the Basque Government and the University of the Basque Country UPV/EHU through of the ENEDI research group for the management and development of the Thermal Area of the Buildings Quality Control Laboratory of the Basque Government (ATLCCE).

Open Access funding provided by University of Basque Country.

References

[1] M. Hazbei, O. Nematollahi, M. Behnia, Z. Adib, Reduction of energy consumption using passive architecture in hot and humid climates, Tunn. Undergr. Space Technol. 47 (2015) 16–27.
[2] B.T. Pan, J. Kao, Comparison of indices for evaluating building green values based on greenhouse gas emission reductions, Ecol. Indicat. 122 (2021), 107228.
[3] R. Widiastuti, J. Zaini, W. Caesarendra, Field measurement on the model of green facade systems and its effect to building indoor thermal comfort, Measurement 166 (2020), 108212.
[4] E. Koroxenidis, T. Theodosiou, Comparative environmental and economic evaluation of green roofs under Mediterranean climate conditions – extensive green roofs a potentially preferable solution, J. Clean. Prod. 311 (2021), 127563.
[5] G. Pérez, L. Rincón, A. Vila, J.M. González, L.F. Cabeza, Green vertical systems for buildings as passive systems for energy savings, Appl. Energy 88 (2011) 4854–4859.
[6] E. Shafiee, M. Faizi, S. Yazdanfar, M. Khanmohammadi, Assessment of the effect of living wall systems on the improvement of the urban heat island phenomenon, Build. Environ. 181 (2020), 106923.
[7] M. Santamouris, Cooling the cities – a review of reflective and green roof mitigation technologies to fight heat island and improve comfort in urban environments, Sol. Energy 103 (2014) 682–703.
[8] S.M. Zaid, E. Perisamy, H. Hussein, N.E. Myeda, N. Zainon, Vertical Greenery System in urban tropical climate and its carbon sequestration potential: a review, Ecol. Indicat. 91 (2018) 57–70.
[9] M. Marchi, R.M. Pulselli, N. Marchettini, F.M. Pulselli, S. Bastianoni, Carbon dioxide sequestration model of a vertical greenery system, Ecol. Model. 306 (2015) 46–56.
[10] Z. Azkorra, G. Pérez, J. Coma, L.F. Cabeza, S. Bures, J.E. Álvaro, et al., Evaluation of green walls as a passive acoustic insulation system for buildings, Appl. Acoust. 89 (2015) 46–56.
[11] R. Thomazelli, F.D.N. Caetano, S.R. Bertoli, Acoustic properties of green walls: absorption and insulation, Proceedings of Meetings on Acoustics Sep 11 (2016) 28DOI.
[12] T. Ysebaert, K. Koch, R. Samson, S. Denys, Green walls for mitigating urban particulate matter pollution—a review, Urban For. Urban Green. 59 (2021), 127014.
[13] J. Khan, K. Kakosimos, S.S. Jensen, O. Hertel, M. Sørensen, J. Gulliver, et al., The spatial relationship between traffic-related air pollution and noise in two Danish cities: implications for health-related studies, Sci. Total Environ. 726 (2020), 138577.
[14] R.W.F. Cameron, J.E. Taylor, M.R. Emmett, What's 'cool' in the world of green façades? How plant choice influences the cooling properties of green walls, Build. Environ. 73 (2014) 198–207.
[15] K.A. Hoffmann, T. Šuklje, J. Kozamernik, T. Nehls, Modelling the cooling energy saving potential of facade greening in summer for a set of building typologies in mid-latitudes, Energy Build. 238 (2021), 110816.
[16] I. Blanco, F. Convertino, E. Schettini, G. Vox, Energy analysis of a green façade in summer: an experimental test in Mediterranean climate conditions, Energy Build. 245 (2021), 111076.
[17] M. Hoelscher, T. Nehls, B. Jänicke, G. Wessolek, Quantifying cooling effects of facade greening: shading, transpiration and insulation, Energy Build. 114 (2016) 283–290.
[18] T. Safikhani, A.M. Abdullah, D.R. Ossen, M. Baharvand, A review of energy characteristic of vertical greenery systems, Renew. Sustain. Energy Rev. 40 (2014) 450–462.
[19] I. Wong, A.N. Baldwin, Investigating the potential of applying vertical green walls to high-rise residential buildings for energy-saving in sub-tropical region, Build. Environ. 97 (2016) 34–39.
[20] M. Dabaieh, A.A. Serageldin, Earth air heat exchanger, Trombe wall and green wall for passive heating and cooling in premium passive refugee house in Sweden, Energy Convers. Manag. 209 (2020), 112555.
[21] S. Sarihi, F. Mehdizadeh Saradj, M. Faizi, A critical review of façade retrofit measures for minimizing heating and cooling demand in existing buildings, Sustain. Cities Soc. 64 (2021), 102525.
[22] P. La Roche, D.J. Yeom, A. Ponce, Passive cooling with a hybrid green roof for extreme climates, Energy Build. 224 (2020), 110243.
[23] H. Omrany, A. Ghaffarianhoseini, A. Ghaffarianhoseini, K. Raahemifar, J. Tookey, Application of passive wall systems for improving the energy efficiency in buildings: a comprehensive review, Renew. Sustain. Energy Rev. 62 (2016) 1252–1269.
[24] R. Djedjig, E. Bozonnet, R. Belarbi, Analysis of thermal effects of vegetated envelopes: integration of a validated model in a building energy simulation program, Energy Build. 86 (2015) 93–103.
[25] M. Kenaï, L. Libessart, S. Lassue, D. Defer, Impact of plants occultation on energy balance: experimental study, Energy Build. 162 (2018) 208–218.
[26] D. Tudiwer, A. Korjenic, The effect of living wall systems on the thermal resistance of the façade, Energy Build. 135 (2017) 10–19.
[27] M. Ottelé, K. Perini, Comparative experimental approach to investigate the thermal behaviour of vertical greened façades of buildings, Ecol. Eng. 108 (2017) 152–161.

[28] J. Coma, G. Pérez, A. de Gracia, S. Burés, M. Urrestarazu, L.F. Cabeza, Vertical greenery systems for energy savings in buildings: a comparative study between green walls and green facades, Build. Environ. 111 (2017) 228–237.
[29] A.B. Daemei, E. Shafiee, A.A. Chitgar, S. Asadi, Investigating the thermal performance of green wall: experimental analysis, deep learning model, and simulation studies in a humid climate, Build. Environ. 205 (2021), 108201.
[30] P. Bano, S. Dervishi, The impact of vertical vegetation on thermal performance of high-rise office building facades in Mediterranean climate, Energy Build. 236 (2021), 110761.
[31] M. Fox, J. Morewood, T. Murphy, P. Lunt, S. Goodhew, Living wall systems for improved thermal performance of existing buildings, Build. Environ. (2021), 108491.
[32] K.J. Kontoleon, E.A. Eumorfopoulou, The effect of the orientation and proportion of a plant-covered wall layer on the thermal performance of a building zone, Build. Environ. 45 (2010) 1287–1303.
[33] M. Kenai, L. Libessart, S. Lassue, D. Defer, Impact of plants obscuration on energy balance: theoretical and numerical study, J. Build. Eng. 29 (2020), 101112.
[34] Y. He, H. Yu, A. Ozaki, N. Dong, S. Zheng, An investigation on the thermal and energy performance of living wall system in Shanghai area, Energy Build. 140 (2017) 324–335.
[35] S. Flores Larsen, C. Filippín, G. Lesino, Modeling double skin green façades with traditional thermal simulation software, Sol. Energy 121 (2015) 56–67.
[36] X. Hao, Q. Xing, P. Long, Y. Lin, J. Hu, H. Tan, Influence of vertical greenery systems and green roofs on the indoor operative temperature of air-conditioned rooms, J. Build. Eng. 31 (2020), 101373.
[37] M. García, S. Vera, F. Rouault, J. Gironás, W. Bustamante, Cooling potential of greenery systems for a stand-alone retail building under semiarid and humid subtropical climates, Energy Build. 259 (2022), 111897.
[38] R. Djedjig, R. Belarbi, E. Bozonnet, Experimental study of green walls impacts on buildings in summer and winter under an oceanic climate, Energy Build. 150 (2017) 403–411.
[39] J. Grieser, B. Rudolf, M. Kottek, C. Beck, F. Rubel, World Map of the Köppen-Geiger climate classification updated, Meteorol. Z. 15 (2006) 259–263.
[40] P.H. Baker, H.A.L. van Dijk, PASLINK and dynamic outdoor testing of building components, Build. Environ. 43 (2008) 143–151.
[41] K.M. Letherman, C.J. Palin, P.M. Park, The measurement of dynamic thermal response in rooms using pseudo-random binary sequences, Build. Environ. 17 (1982) 11–16.
[42] G.P. van der Linden, H.A.L. van Dijk, A.J. Lock, F. van der Graaf, COMPASS Installation Guide HFS Tiles for the PASSYS Test Cells, 1995.
[43] PASSYS, Operations Manual, 1993.
[44] H.A.L. van Dijk, G.P. van der Linden, PASLINK Calibration and Component Test Procedures, 1995.
[45] M. Köhler, Green facades—a view back and some visions, Urban Ecosyst. 11 (2008) 423–436.
[46] C. Bolton, M.A. Rahman, D. Armson, A.R. Ennos, Effectiveness of an ivy covering at insulating a building against the cold in Manchester, U.K: a preliminary investigation, Build. Environ. 80 (2014) 32–35.
[47] N.R. Kristensen, H. Madsen, Continuous Time Stochastic Modelling. CTSM 2.3—user's Guide, Technical University of Denmark, 2003.
[48] I. Naveros, P. Bacher, D.P. Ruiz, M.J. Jiménez, H. Madsen, Setting up and validating a complex model for a simple homogeneous wall, Energy Build. 70 (2014) 303–317.
[49] Q. Chen, B. Li, X. Liu, An experimental evaluation of the living wall system in hot and humid climate, Energy Build. 61 (2013) 298–307.
[50] F. Convertino, G. Vox, E. Schettini, Evaluation of the cooling effect provided by a green façade as nature-based system for buildings, Build. Environ. 203 (2021), 108099.
[51] R. Sendra-Arranz, V. Oquendo, L. Olivieri, F. Olivieri, C. Bedoya, A. Gutiérrez, Monitorization and statistical analysis of south and west green walls in a retrofitted building in Madrid, Build. Environ. 183 (2020), 107049.
[52] N.H. Wong, A.Y. Kwang Tan, Y. Chen, K. Sekar, P.Y. Tan, D. Chan, et al., Thermal evaluation of vertical greenery systems for building walls, Build. Environ. 45 (2010) 663–672.
[53] E. Cuce, Thermal regulation impact of green walls: an experimental and numerical investigation, Appl. Energy 194 (2017) 247–254.
[54] G. Pérez, L. Rincón, A. Vila, J.M. González, L.F. Cabeza, Behaviour of green facades in Mediterranean Continental climate, Energy Convers. Manag. 52 (2011) 1861–1867.